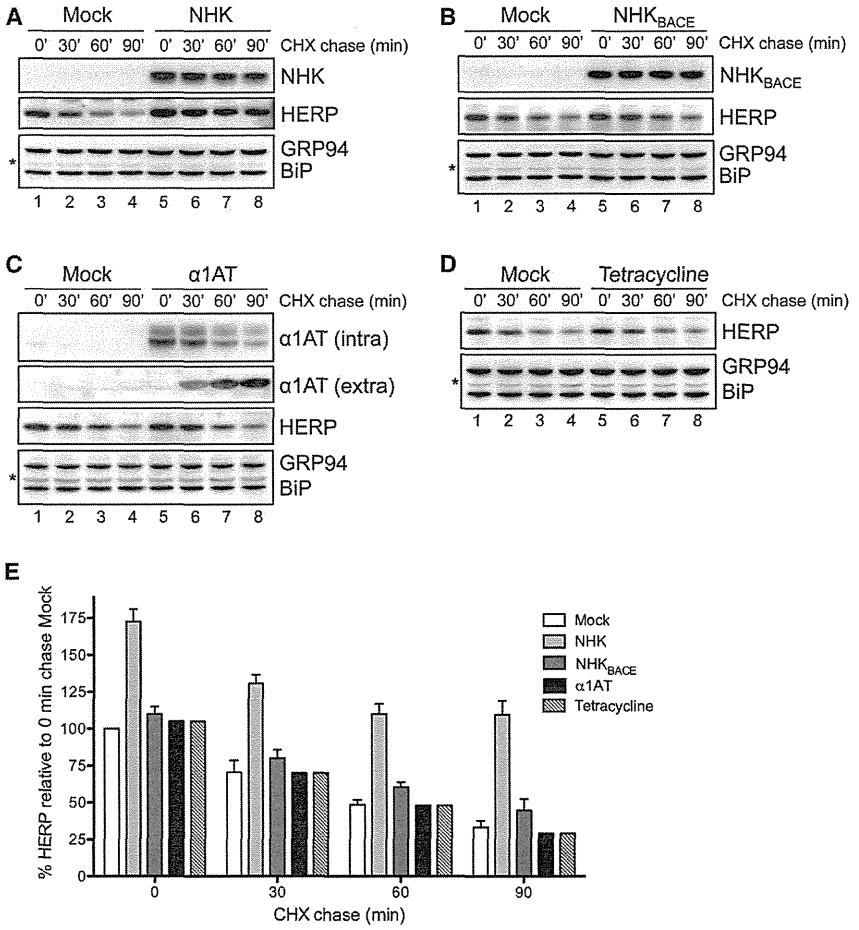

Figure 4. NHK Expression Delays HERP Turnover

(A) HERP turnover (second panel) was analyzed by CHX chase in cells not induced (lanes 1–4, first panel) or induced for expression of the misfolded protein NHK (lanes 5–8, first panel, induction with 100 ng/ml tetracycline for 5 hr) and quantified (E). The asterisk shows a cross-reacting protein.

(B) Same as (A) for the misfolded protein NHK_{BACE}.

(C) Same as (A) for the native protein α1AT. Intra, intracellular; extra, extracellular.

(D) Same as (A) for mock cells not incubated or incubated with tetracycline.

(E) HERP levels in (A)–(D) were quantified relative to 0 min CHX chase mock and plotted. Error bars: SD from the mean of three replicates.

(Figure 4A, lanes 1–4) or in the presence of tetracycline to induce NHK expression (lanes 5–8). Western blot analysis of the cell lysates showed that in cells expressing NHK, the HERP turnover was substantially slower ($t_{1/2}$ > 120 min; Figures 4A, second panel, lanes 5–8, and 4E, NHK) than in cells not expressing the HRD1 client ($t_{1/2}$ of 60 min; Figures 4A, second panel, lanes 1–4, and 4E, mock). Confirming the data shown in Figure 3, the NHK-induced delay in HERP turnover did increase the intraluminal level of the endogenous protein so that at steady state, the level of endogenous HERP in cells expressing NHK was 1.7 times higher than that in cells not expressing NHK (Figures 4A, second panel, lanes 5 versus 1, and 4E, NHK versus mock), and after a 90 min CHX chase it was 4 times higher (Figure 4E, NHK versus mock). Similar results were obtained in cells expressing κ-LC (Figure S5), another HERP/HRD1 client (Okuda-Shimizu and Hendershot, 2007).

NHK_{BACE} displays the same luminal misfolded domain of NHK, but it is anchored at the ER membrane (i.e., it is an ERAD-L_M substrate, Figure S3). Anchorage of ERAD substrates at the membrane renders them more promiscuous in the engagement of ERAD pathways for efficient disposal (Bernasconi et al., 2010a; 2010b; Ninagawa et al., 2011). Consistent with a less stringent engagement of the HRD1 pathway, silencing of HERP expression did not significantly affect NHK_{BACE} degradation (Figures S4C and S4D). NHK_{BACE} expression only marginally delayed HERP turnover (Figures 4B and 4E) and did not significantly affect the intraluminal level of HERP (Figures 4B, second panel, lanes 5 versus 1, and 4E, NHK_{BACE} versus mock). Likewise, expression of the folding-competent protein α1AT (Figures 4C, 4E, and S3) or cell exposure to tetracycline, which is used to induce transgene expression (Figures 4D and 4E), did not affect HERP stability or levels.

Altogether, these data reveal that HRD1 clients elicit an autoadaptive regulatory response that anticipates UPR induction to rapidly enhance the intracellular level of HERP by stabilizing its association with components of the HRD1 dislocon, thereby inhibiting its UPS-regulated constitutive turnover.

Separation of HERP Complexes in Sucrose Density Gradients

The yeast ortholog Usa1p regulates assembly and activity of the HRD1 dislocon (Carroll and Hampton, 2010; Carvalho et al., 2006; 2010; Horn et al., 2009; Kanehara et al., 2010; Kim et al., 2009). Usa1p- and HERP-containing complexes can be analyzed in sedimentation gradients (Carvalho et al., 2006; 2010; Horn et al., 2009; Iida et al., 2011; Kny et al., 2011). Since NHK expression delays the turnover of endogenous HERP, thus increasing its intracellular level (Figures 3 and 4), we next verified whether expression of this misfolded HRD1 client affects the stability of the pool of endogenous HERP participating in the supramolecular complexes dedicated to ERAD substrate dislocation across the ER membrane.

To this end, we set up a protocol for differential sedimentation of endogenous HERP excluded from or included into the HERP-SEL1L-HRD1-DER1 dislocon in cells expressing or not expressing NHK. HEK293 cells were lysed in CHAPS, a zwitterionic detergent that preserves multimeric protein complexes. Insoluble material was removed by centrifugation, and the soluble fraction of the cell lysates was loaded at the top of a linear

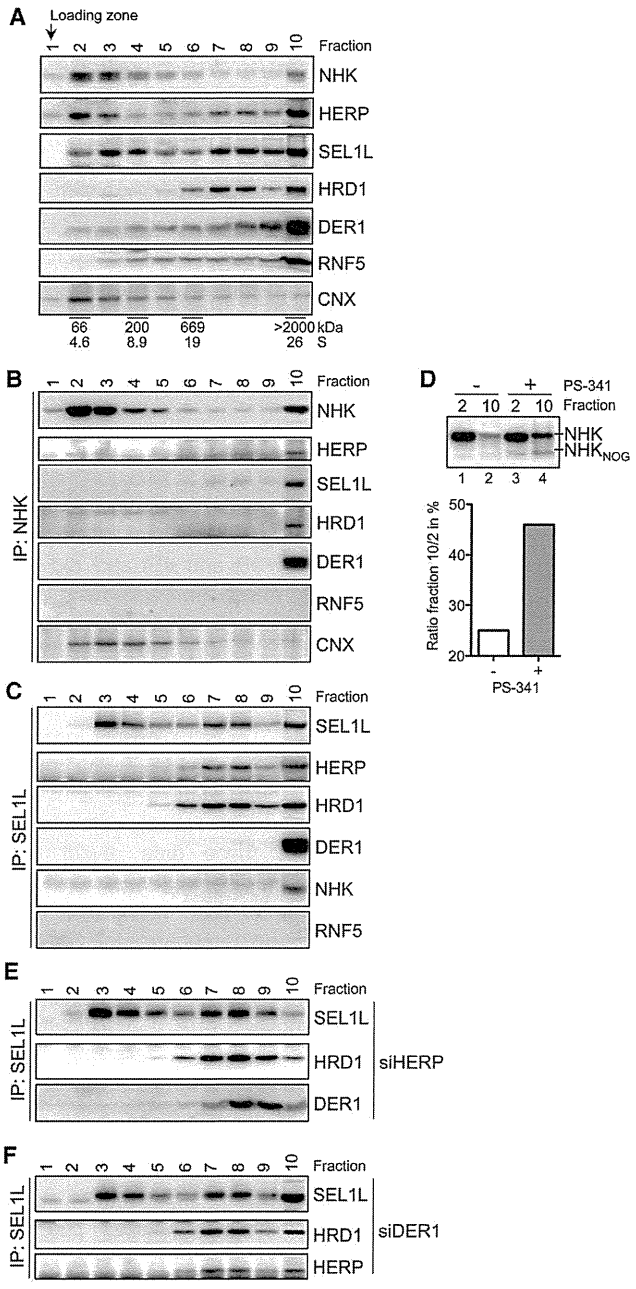

Figure 5. HRD1 Dislocon Analysis in Sucrose Density Gradients

(A) Sedimentation of NHK (induction with 10 ng/ml tetracycline for 16 hr), endogenous HERP, SEL1L, HRD1, DER1, RNF5, and CNX in sucrose gradients (western blot). Sedimentation of standards is shown.

(B) NHK was immunoisolated from each fraction (first panel), and the associated HERP, SEL1L, HRD1, DER1, RNF5, and CNX were detected by western blot.

(C) Same as in (B) for SEL1L.

(D) Level of NHK in fractions 2 or 10 in mock (lanes 1 and 2) or in cells treated with PS-341 for 4 hr (lanes 3 and 4) was assessed by western blot. Note the appearance of the degradation intermediate deglycosylated NHK (NHK$_{NOG}$) in fraction 10 upon proteasomal inhibition (lane 4). The level of NHK in fraction 10 relative to fraction 2 was quantified and plotted.

(E) Same as in (C) in siHERP cells not expressing NHK.

(F) Same as in (E) in siDER1 cells. Analysis of the gradients has been repeated 6, 3, 2, 2, 2, and 2 times, respectively.

sucrose gradient (10%–60%; Figures 5, S6, and S7, and Experimental Procedures). After sample ultracentrifugation, 10 fractions were collected from the top (the position of sedimentation markers is shown in Figure 5A). Western blot analysis showed that the ERAD substrate NHK was mainly distributed in fractions 2–4 and 10. Endogenous HERP and SEL1L were separated in three major pools sedimenting in fractions 2–4, 7–8, and 10. HRD1 was in two major pools in fractions 7–8 and 10. DER1 and RNF5 were mostly found in fraction 10, and CNX was mostly found in fractions 2–4 (Figure 5A).

Identification of Active Dislocation Complexes Containing the HRD1 Client NHK

Immunoisolation of NHK from the sucrose gradient fractions (Figure 5B) and detection of the interacting proteins by western blot showed that in fractions 2–4, NHK was physically associated with CNX, an ER-resident lectin chaperone that assists folding-defective polypeptides during the unsuccessful attempts to attain the native structure (Molinari et al., 2002), but not with endogenous HERP and SEL1L sedimenting in the same fractions (Figures 5A and 5B). In contrast, NHK in fraction 10 was in large complexes containing all major components of the HRD1 dislocation machinery, as shown by the presence of HERP, SEL1L, HRD1, DER1, and NHK in the same immunocomplexes (Figures 5B and 5C). RNF5 does not participate in the HRD1 dislocon complex (Christianson et al., 2012). Consistently, it did not coprecipitate with the HRD1 client NHK (Figure 5B) or with other components of the HRD1 dislocon coimmunoisolated from fraction 10 (Figure 5C). Altogether, these data and the fact that NHK accumulated in fraction 10 upon inhibition of proteasomal activity (Figure 5D) led us to conclude that this fraction contains active dislocons engaged by HRD1 clients for retrotranslocation across the ER membrane. Incomplete dislocons lacking DER1 and NHK (Figures 5B and 5C), as well as the HERP:RNF5 complexes whose formation regulates the constitutively fast turnover of HERP (Figures 2H and S6A), sediment in lighter fractions of the sucrose gradients (i.e., fractions 6–8).

Smaller HRD1 Dislocons in Cells Containing Reduced Levels of Endogenous HERP

In *S. cerevisiae*, Usa1p ensures the clustering of Hrd1p/Hrd3p/Der1p-containing oligomers in higher-order functional complexes (Carvalho et al., 2010; Horn et al., 2009). Consistent with evolutionary conservation of this function in the mammalian system, silencing HERP expression (siHERP; Figure S6B) caused a sedimentation shift of SEL1L-, HRD1-, and DER1-containing complexes from fraction 10 (Figures 5A–5C and S6D; for cells treated with a scrambled small interfering RNA [siSCR]) to fractions 7 and 8 (Figures 5E, S6D, and S6F; siHERP). This corresponds to a reduction in HRD1 dislocon size from more than 2,000 kDa (>26S) to approximately 700 kDa (19S). As reported for yeast, such a reduction cannot be explained by the absence of HERP alone. Consistently, DER1 silencing (Figure S6C), which does not affect clustering of Hrd1 dislocons in

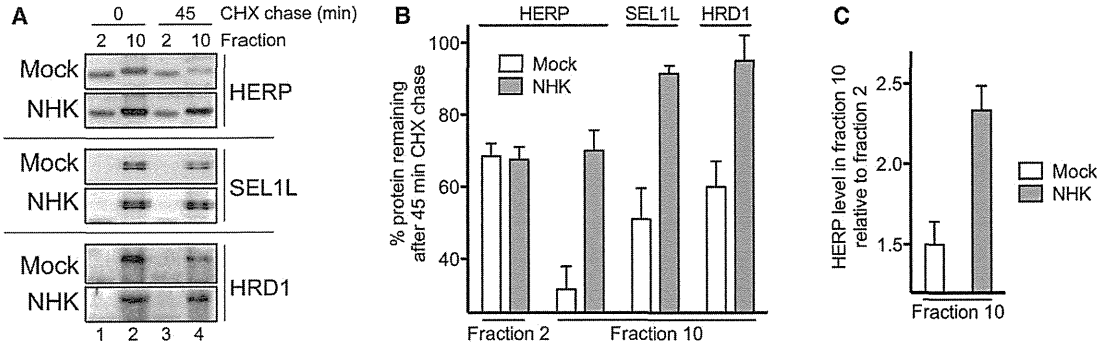

Figure 6. Substrate-Induced Stabilization of the HRD1 Dislocon-Associated HERP and of the HRD1 Dislocon

(A) HERP turnover in fractions 2 or 10 (first and second panels) and stability of SEL1L- (third and fourth panels) or HRD1-containing complexes (fifth and sixth panels) in fraction 10 monitored by CHX chase in cells not induced (mock) or induced for 16 hr with 10 ng/ml tetracycline (NHK) for expression of NHK.

(B) Quantification of remaining HERP in fraction 2 and HERP, SEL1L, and HRD1 in fraction 10 after 45 min CHX chase in mock (white columns) or in cells expressing NHK (gray columns).

(C) HERP levels in fraction 10 at steady state (0 min CHX chase; Figure 6A, first and second panels, lane 2) in mock (white columns) and in cells expressing NHK (gray columns) were quantified relative to fraction 2 (Figure 6A, first and second panels, lane 1) and plotted. Error bars: SD from the mean of two replicates.

yeast (Horn et al., 2009), did not significantly change the sedimentation of complexes containing HERP, SEL1L, and HRD1 (Figures 5F and S6D, siDER1). Upon HERP silencing, NHK did not sediment in fraction 10 (Figure S6E, to be compared with NHK distribution in the sucrose gradient of wild-type cell extracts in Figure 5B), it did not associate with components of fragmented HRD1 dislocons in fractions 7–9 (Figures S6E and S6F versus Figures 5B and 5C), and its disposal from the ER was substantially delayed (Figures S4A and S4B).

Expression of the HRD1 Client NHK Specifically Stabilizes HERP and the HRD1 Dislocon

HERP is subjected to constitutively rapid turnover, which is delayed upon luminal expression of the HRD1 client NHK (Figures 3 and 4). In sucrose gradients, only endogenous HERP sedimenting in fraction 10 is engaged in complexes with all major components of the HRD1 dislocation machinery and with the HRD1 client to be dislocated across the ER membrane (Figure 5). To test whether HRD1 clients stabilize HERP in the HRD1 dislocon, the turnover of the pool of endogenous HERP excluded from the HRD1 dislocon (fraction 2) was compared with the turnover of HERP engaged in the active HRD1 dislocation machinery (fraction 10). A CHX chase analysis revealed that the pool of endogenous HERP in fraction 2 was relatively stable (35% decay in 45 min; Figures 6A, first panel, lanes 1 versus 3, and 6B, mock, white column). The decay of this pool of HERP was not affected upon induction of NHK expression (Figures 6A, second panel, lanes 1 versus 3, and 6B, NHK, gray column). In contrast, the pool of endogenous HERP engaged in the HRD1 dislocon (fraction 10) was unstable at steady state (65% decay in 45 min; Figures 6A, first panel, lanes 2 versus 4, and 6B, mock, white column) and was substantially stabilized upon expression of NHK (only 25% decay in 45 min; Figures 6A, second panel, lanes 2 versus 4, and 6B, NHK, gray column). Consistent with a client-induced stabilization of endogenous HERP in the HRD1 dislocon, the level of HERP in fraction 10 relative to the free pool in fraction 2 substantially increased upon induction of NHK expression (Figures 6A, lane 2, first versus second panel, and 6C).

In contrast to HERP, the other components of the HRD1 dislocon are stable proteins (Cambridge et al., 2011). Consistently, the intracellular levels of SEL1L and HRD1 that have half-lives of 26 and 37 hr, respectively (Figure S7A) (Cambridge et al., 2011), did not change during the 45 min of chase of the experiment shown in Figure 6A. Nevertheless, the fraction of SEL1L and HRD1 in the active dislocons sedimenting in fraction 10 was reduced by 35% and 50%, respectively, during a 45 min chase (Figures 6A, third and fifth panel, lanes 4 versus 2, and 6B, SEL1L and HRD1, white columns) and even more after longer CHX chase that fully depletes endogenous HERP (180 min in Figure S7B). Under these conditions, the HRD1 dislocons disassemble, and the sedimentation of SEL1L-, HRD1-, and DER1-containing complexes shifted from fraction 10 (>2,000 kDa/26S; Figure S7B) to fractions 7–8, corresponding to an approximate size of 700 kDa/19S (Figure S7B). Based on these data, the half-life of HRD1 dislocation machineries can be estimated to be less than 60 min at steady state.

Induction of expression of the HRD1 client NHK, shown above to stabilize HERP, also stabilized the dislocon machinery, as shown by the persistency of SEL1L and HRD1 in the large complexes sedimenting in fraction 10 (Figures 6A, fourth and sixth panels, lanes 4 versus 2, and 6B, SEL1L and HRD1, gray columns). This is consistent with a model in which the engagement of HRD1 dislocons by clients maintains their integrity and stabilizes HERP, thus insuring autoadaptive mechanisms that allow rapid and client-specific adjustments of ERAD activity to variations in misfolded polypeptide load in the ER lumen.

DISCUSSION

Mammalian cells deploy a constitutive ERAD activity that must cope with the physiologic byproducts of protein biogenesis, generated by the intrinsic inefficiency of protein folding programs in the ER lumen. This study reveals an autoadaptive mechanism whereby the ERAD machinery rapidly responds to fluctuations in misfolded clients to be dislocated across the ER membrane for proteasomal degradation. The response consists

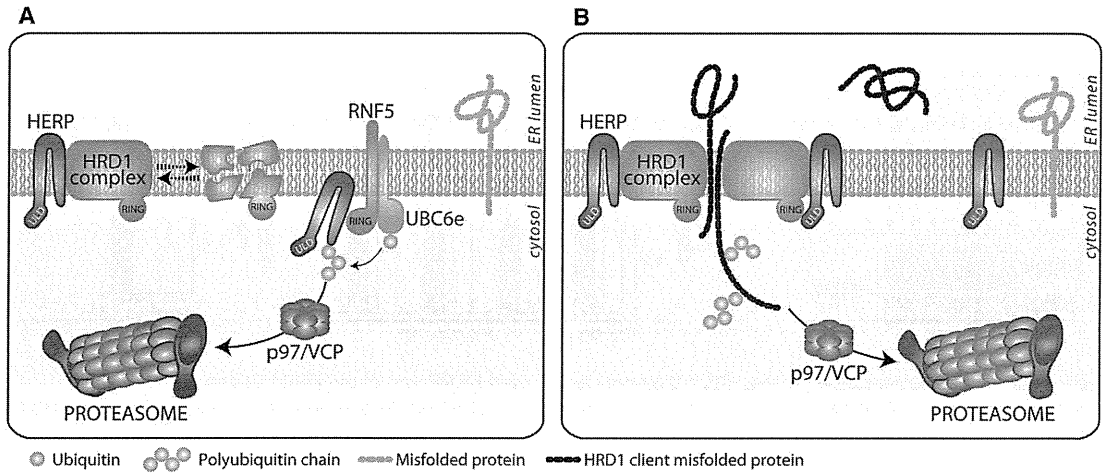

Figure 7. Client-Dependent Regulated HERP Turnover and HRD1 Dislocon Integrity

(A) ERAD tuning constitutively adapts ERAD activity regulating segregation from the folding compartment of select ERAD factors and their disengagement from active ERAD complexes (Bernasconi et al., 2012a). HRD1 dislocons are unstable when not engaged by clients. As a consequence, the linchpin protein HERP is degraded by the action of UBC6e, RNF5, p97, and the 26S proteasome.

(B) Misfolded polypeptides affect ERAD tuning mechanisms to boost ERAD activity. Expression of HRD1 clients recruits and stabilizes the HRD1 dislocons by interfering with the RNF5-dependent HERP recognition and removal. The increased stability of HERP stabilizes, in turn, the whole HRD1 dislocation machinery. RING, really interesting new gene finger domain (catalytic domain); ULD, ubiquitin-like domain.

of a client-induced stabilization of HRD1 dislocons and of HERP, a crucial regulator of HRD1 dislocon assembly and activity (Figure 7). Both the dislocons and HERP are intrinsically unstable when not engaged by misfolded polypeptides. We propose that autoadaptive ERAD is the first line of defense to contrast accumulation of misfolded polypeptides, preceding and possibly preventing activation of transcriptional UPR programs.

Cumulative data highlight the role of misfolded polypeptides in directly determining ERAD activity (the ERAD tuning model; Bernasconi and Molinari, 2011; Leitman et al., 2013; Merulla et al., 2013). For example, misfolded polypeptides may act as preferred acceptors for the ubiquitylating activity of membrane-embedded E3 ubiquitin ligases, thereby competing with the heterologous ubiquitylation and self-ubiquitylation shown to constitutively clear from the ER membrane or inactivate E3 ubiquitin ligases such as SURF1, RFP2, and gp78 (Ballar et al., 2010; Guo et al., 2011; Lerner et al., 2007; Shmueli et al., 2009; Weissman et al., 2011). Moreover, folding-defective clients of specific ERAD pathways may specifically ensure maintenance of the integrity of functional ERAD complexes (Bernasconi et al., 2012a; Calì et al., 2008; Nakatsukasa et al., 2013; Reggiori et al., 2010) and of supramolecular dislocation machineries (this study). By inhibiting the disassembly that occurs when dislocation machineries are unengaged (this study), misfolded proteins may also inhibit the segregation of ERAD factors such as SEL1L, EDEM1, and OS-9 in ER-derived vesicles or in ER subdomains (Bernasconi et al., 2012a; Calì et al., 2008). Interestingly, these ER-derived subdomains are eventually coopted by arteritis and coronaviruses to become platforms for viral genome replication as an indication that ERAD tuning pathways might be hijacked by pathogens to promote infection (Bernasconi et al., 2012b; Monastyrska et al., 2013; Reggiori et al., 2010). Finally, misfolded polypeptides have been shown to interfere with the polyubiquitylation of the membrane protein JAMP, thereby promoting recruitment of 26S proteasomes at the ER membrane (Tcherpakov et al., 2009). In all of these ERAD tuning responses, the expression of misfolded polypeptides enhances ERAD activity directly and immediately. We propose that only when autoadaptive ERAD capacity is overwhelmed by the misfolded protein load might the consequent perturbations in the ER folding environment possibly decoded by the luminal reduction of free BiP activate the conventional UPR, causing ER swelling, enhanced synthesis of ER-resident folding and degradation regulators, and attenuation of cargo proteins production. We speculate that the avidity of the given misfolded polypeptide for BiP may determine the threshold for UPR activation. In other words, substrates with a high capacity for BiP binding may elicit the transition between ERAD tuning response and transcriptional UPR at lower expression levels than polypeptides that bind less BiP.

ERAD tuning responses are more rapidly triggered than UPR, whose onset has a latency of several hours (Pincus and Walter, 2012; Walter and Ron, 2011), and are more readily reversible. Their reversibility relies in fact on the reactivation of the constitutively rapid turnover, removal from the ER, and/or removal from functional ERAD complexes of select ERAD factors that occurs at low doses of misfolded polypeptides when dislocons are empty and are, at least partly, disassembled. In contrast, the recovery from a UPR requires activation of elusive mechanisms that reduce the size of the ER after the UPR-triggered expansion and that remove the excess of chaperones produced during the ER stress phase, most of which have half-lives exceeding 24 hr (Cambridge et al., 2011).

The ER membrane contains at least 24 RING finger E3 ubiquitin ligases (Neutzner et al., 2011). Few of them have a

documented role in the clearance of aberrant gene products from the ER, are engaged by misfolded polypeptides with different physicochemical features, and enter supramolecular complexes with specific composition that, in some cases, share common components (Brodsky and Wojcikiewicz, 2009; Christianson et al., 2012; Merulla et al., 2013). The organization of ERAD as a dynamic network of interacting functional modules that efficiently cope with the production of diverse classes of misfolded polypeptides has been proposed (Christianson et al., 2012). It is a matter of further investigations to understand whether the client-dependent regulation mechanisms shown to operate for the HRD1 pathway also exist to regulate other dislocation machineries and other ERAD pathways. If this is the case, one could envision that cellular proteostasis is not maintained by pleiotropic and/or nonspecific adaptations of ERAD activity to the compartmental load with misfolded cargo. Rather, selective activation of dedicated pathways and assembly of the relevant modules would allow rapid and specific responses to the species of aberrant gene products that cells are challenged with. We suggest that defective "ERAD elasticity" (i.e., the reduced capacity to efficiently cope with fluctuations in misfolded polypeptide load by activating ERAD tuning responses that preempt UPR induction) could be a reason for increased sensitivity to misfolded protein load in aging cells and tissues, possibly resulting in the onset and/or progression of conformational diseases.

EXPERIMENTAL PROCEDURES

Cell Lines, CHX Chase, RNAi, and Flp-In T-REx HEK293 Inducible Cell Line

HEK293 and HeLa cells were grown in Dulbecco's modified Eagle's medium (DMEM) or in modified Eagle's medium alpha (MEMα), respectively, supplemented with 10% fetal bovine serum (FBS). For HERP turnover analysis, cells at 80%–90% confluence were incubated with 50 μg/ml CHX (Sigma) for the indicated times. At the end of the chase, cells were lysed in ice-cold lysis buffer (2% CHAPS [Anatrace] in HEPES-buffered saline [HBS; pH 6.8], 20 mM N-ethylmaleimide, and protease inhibitors). Proteins of interest were detected by western blot as explained below. For siRNA-based interference, HeLa or HEK293 cells at 50% confluence in a 3.5 cm tissue culture plate were transfected with siRNA duplex (from QIAGEN or Ambion; 50 pmol/dish; Table S1A) using Lipofectamine 2000 (Invitrogen). Experiments were performed 48 hr after transfection. Stable inducible HEK293 cells expressing the gene of interest have been generated using the Flp-In T-REx system (Invitrogen) following the instructions of the manufacturer. Transgene expression was induced by supplementing the cell culture medium with 0–100 ng/ml tetracycline (Sigma) as specified for each figure.

Antibodies and Inhibitors

The following antibodies were used: CNX, gp78, HRD1, RNF5, and UBC6e (kind gifts of A. Helenius, S. Fang, R. Wojcikiewicz, Z. Ronai, and H. Ploegh, respectively); HERP (Kokame et al., 2000); HA, DER1, HERP, RNF5, and SEL1L (Sigma); ERp72, KDEL (Stressgen); actin (Santa Cruz); tubulin (Applied Biological Materials); ubiquitin (DAKO). PS-341 (Millennium Pharmaceuticals), CQ, DBeQ, and CHX (Sigma) have been used at final concentrations of 10 μM, 100 μM, 10 or 15 μM, and 50 μg/ml, respectively.

Metabolic Labeling, Immunoprecipitations, Western Blots, and Analysis of Data

HeLa or HEK293 cells were pulsed with 0.05 mCi [^{35}S]methionine/cysteine mix and chased for the indicated times with DMEM supplemented with 5 mM cold methionine and cysteine. Postnuclear supernatant (PNS) was prepared by solubilization of cells in lysis buffer. Native immunoprecipitations were performed by adding protein A beads (Sigma; 1:10, w/v swollen in 50 mM HEPES, 200 mM NaCl [HBS]) with the select antibody and incubated for 2 hr at 4°C. Immunoprecipitates were extensively washed (3 times for 10 min each) with 0.5% CHAPS in HBS, resuspended in sample buffer, incubated at 65°C for 10 min, and finally separated in SDS-PAGE. To assess the polyubiquitylation level of HERP, HERP-containing complexes were disrupted by lysing cells with RIPA buffer. Immunoprecipitates were extensively washed with 0.5% Triton in HBS. Protein transfer was performed with the Trans-Blot Turbo Transfer System (Bio-Rad). Western blots were performed using the SNAP i.d. system (Millipore). The Luminata Forte ECL detection system was from Millipore, and signals were detected using ImageQuant LAS 4000 system (GE Healthcare, Life Sciences). Quantifications using the MultiGauge analysis software were performed in the linear range of the western blot signal (Figure S2B).

Semiquantitative and Quantitative RT-PCR

Total RNA was isolated using the GenElute Mammalian Total RNA Miniprep Kit (Sigma) according to the instructions of the manufacturer. A total of 2 μg of RNA was used for cDNA synthesis using SuperScript II Reverse Transcriptase and Oligo(dT) (Invitrogen). RT-PCR was performed using *Taq* DNA Polymerase (Invitrogen) with transcript-specific primers (Table S1B). Quantitative RT-PCR was performed using 7900HT Fast Real-Time PCR System. The PCR reactions were performed using the Power SYBR Green PCR Master Mix (Applied Biosystems). The housekeeping gene β-actin was used as reference. Data were analyzed using the SDS 2.2.2 software.

Sucrose Density Gradient Centrifugation

HEK293 cells in a 6 cm dish were solubilized in 0.4 ml lysis buffer and centrifuged at 10,000 rpm for 10 min. PNS was collected and applied to a 10%–60% linear sucrose gradient (in 2% CHAPS-HBS [pH 6.8]) prepared with a Gradient Master BioComp. Separation of the intracellular protein complexes was performed by ultracentrifugation in a MLS-50 rotor (16 hr, 157,000 × *g*, 4°C). Fractions (0.5 ml) were collected from the top. Standards are as follows: BSA (66 kDa, 4.6S), β-amylase (200 kDa, 8.9S), and porcine thyroid thyroglobulin (669 kDa, 19S). For immunoprecipitations, fractions were diluted 5× with lysis buffer.

Statistical Analysis

Independent experiments were quantified, analyzed with the Prism 5 software, and plotted as the mean ± SD.

SUPPLEMENTAL INFORMATION

Supplemental Information includes Supplemental Experimental Procedures, seven figures, and one table and can be found with this article online at http://dx.doi.org/10.1016/j.molcel.2013.10.016.

ACKNOWLEDGMENTS

We thank T. Beltraminelli, G. Codoni, and E. Fasana for technical help; S. Fang, R. Geiger, A. Helenius, H. Ploegh, Z. Ronai, R. Wojcikiewicz, and Y. Ye for various reagents; L. Humpert, P. Paganetti, E. van Anken, and members of the M.M. lab for critical reading the manuscript. M.M. is supported by Signora Alessandra, the Foundation for Research on Neurodegenerative Diseases, the Swiss National Science Foundation, the Association Française contre les Myopathies, and the Gabriele Foundation.

Received: July 3, 2013
Revised: September 23, 2013
Accepted: October 9, 2013
Published: November 14, 2013

REFERENCES

Balch, W.E., Morimoto, R.I., Dillin, A., and Kelly, J.W. (2008). Adapting proteostasis for disease intervention. Science *319*, 916–919.

Ballar, P., Ors, A.U., Yang, H., and Fang, S. (2010). Differential regulation of CFTRDeltaF508 degradation by ubiquitin ligases gp78 and Hrd1. Int. J. Biochem. Cell Biol. *42*, 167–173.

Bernasconi, R., and Molinari, M. (2011). ERAD and ERAD tuning: disposal of cargo and of ERAD regulators from the mammalian ER. Curr. Opin. Cell Biol. *23*, 176–183.

Bernasconi, R., Pertel, T., Luban, J., and Molinari, M. (2008). A dual task for the Xbp1-responsive OS-9 variants in the mammalian endoplasmic reticulum: inhibiting secretion of misfolded protein conformers and enhancing their disposal. J. Biol. Chem. *283*, 16446–16454.

Bernasconi, R., Galli, C., Calanca, V., Nakajima, T., and Molinari, M. (2010a). Stringent requirement for HRD1, SEL1L, and OS-9/XTP3-B for disposal of ERAD-LS substrates. J. Cell Biol. *188*, 223–235.

Bernasconi, R., Soldà, T., Galli, C., Pertel, T., Luban, J., and Molinari, M. (2010b). Cyclosporine A-sensitive, cyclophilin B-dependent endoplasmic reticulum-associated degradation. PLoS ONE *5*, e13008.

Bernasconi, R., Galli, C., Noack, J., Bianchi, S., de Haan, C.A., Reggiori, F., and Molinari, M. (2012a). Role of the SEL1L:LC3-I complex as an ERAD tuning receptor in the mammalian ER. Mol. Cell *46*, 809–819.

Bernasconi, R., Noack, J., and Molinari, M. (2012b). Unconventional roles of nonlipidated LC3 in ERAD tuning and coronavirus infection. Autophagy *8*, 1534–1536.

Braakman, I., and Hebert, D.N. (2013). Protein folding in the endoplasmic reticulum. Cold Spring Harb. Perspect. Biol. *5*, a013201.

Brodsky, J.L. (2012). Cleaning up: ER-associated degradation to the rescue. Cell *151*, 1163–1167.

Brodsky, J.L., and Wojcikiewicz, R.J. (2009). Substrate-specific mediators of ER associated degradation (ERAD). Curr. Opin. Cell Biol. *21*, 516–521.

Calì, T., Galli, C., Olivari, S., and Molinari, M. (2008). Segregation and rapid turnover of EDEM1 by an autophagy-like mechanism modulates standard ERAD and folding activities. Biochem. Biophys. Res. Commun. *371*, 405–410.

Cambridge, S.B., Gnad, F., Nguyen, C., Bermejo, J.L., Krüger, M., and Mann, M. (2011). Systems-wide proteomic analysis in mammalian cells reveals conserved, functional protein turnover. J. Proteome Res. *10*, 5275–5284.

Carroll, S.M., and Hampton, R.Y. (2010). Usa1p is required for optimal function and regulation of the Hrd1p endoplasmic reticulum-associated degradation ubiquitin ligase. J. Biol. Chem. *285*, 5146–5156.

Carvalho, P., Goder, V., and Rapoport, T.A. (2006). Distinct ubiquitin-ligase complexes define convergent pathways for the degradation of ER proteins. Cell *126*, 361–373.

Carvalho, P., Stanley, A.M., and Rapoport, T.A. (2010). Retrotranslocation of a misfolded luminal ER protein by the ubiquitin-ligase Hrd1p. Cell *143*, 579–591.

Chou, T.F., Brown, S.J., Minond, D., Nordin, B.E., Li, K., Jones, A.C., Chase, P., Porubsky, P.R., Stoltz, B.M., Schoenen, F.J., et al. (2011). Reversible inhibitor of p97, DBeQ, impairs both ubiquitin-dependent and autophagic protein clearance pathways. Proc. Natl. Acad. Sci. USA *108*, 4834–4839.

Christianson, J.C., Shaler, T.A., Tyler, R.E., and Kopito, R.R. (2008). OS-9 and GRP94 deliver mutant alpha1-antitrypsin to the Hrd1-SEL1L ubiquitin ligase complex for ERAD. Nat. Cell Biol. *10*, 272–282.

Christianson, J.C., Olzmann, J.A., Shaler, T.A., Sowa, M.E., Bennett, E.J., Richter, C.M., Tyler, R.E., Greenblatt, E.J., Harper, J.W., and Kopito, R.R. (2012). Defining human ERAD networks through an integrative mapping strategy. Nat. Cell Biol. *14*, 93–105.

Eura, Y., Yanamoto, H., Arai, Y., Okuda, T., Miyata, T., and Kokame, K. (2012). Derlin-1 deficiency is embryonic lethal, Derlin-3 deficiency appears normal, and Herp deficiency is intolerant to glucose load and ischemia in mice. PLoS ONE *7*, e34298.

Gao, H., Wang, Y., Wegierski, T., Skouloudaki, K., Pütz, M., Fu, X., Engel, C., Boehlke, C., Peng, H., Kuehn, E.W., et al. (2010). PRKCSH/80K-H, the protein mutated in polycystic liver disease, protects polycystin-2/TRPP2 against HERP-mediated degradation. Hum. Mol. Genet. *19*, 16–24.

Greenblatt, E.J., Olzmann, J.A., and Kopito, R.R. (2011). Derlin-1 is a rhomboid pseudoprotease required for the dislocation of mutant α-1 antitrypsin from the endoplasmic reticulum. Nat. Struct. Mol. Biol. *18*, 1147–1152.

Guo, X., Shen, S., Song, S., He, S., Cui, Y., Xing, G., Wang, J., Yin, Y., Fan, L., He, F., and Zhang, L. (2011). The E3 ligase Smurf1 regulates Wolfram syndrome protein stability at the endoplasmic reticulum. J. Biol. Chem. *286*, 18037–18047.

Hori, O., Ichinoda, F., Yamaguchi, A., Tamatani, T., Taniguchi, M., Koyama, Y., Katayama, T., Tohyama, M., Stern, D.M., Ozawa, K., et al. (2004). Role of Herp in the endoplasmic reticulum stress response. Genes Cells *9*, 457–469.

Horn, S.C., Hanna, J., Hirsch, C., Volkwein, C., Schütz, A., Heinemann, U., Sommer, T., and Jarosch, E. (2009). Usa1 functions as a scaffold of the HRD-ubiquitin ligase. Mol. Cell *36*, 782–793.

Hosokawa, N., Wada, I., Nagasawa, K., Moriyama, T., Okawa, K., and Nagata, K. (2008). Human XTP3-B forms an endoplasmic reticulum quality control scaffold with the HRD1-SEL1L ubiquitin ligase complex and BiP. J. Biol. Chem. *283*, 20914–20924.

Iida, Y., Fujimori, T., Okawa, K., Nagata, K., Wada, I., and Hosokawa, N. (2011). SEL1L protein critically determines the stability of the HRD1-SEL1L endoplasmic reticulum-associated degradation (ERAD) complex to optimize the degradation kinetics of ERAD substrates. J. Biol. Chem. *286*, 16929–16939.

Kanehara, K., Xie, W., and Ng, D.T. (2010). Modularity of the Hrd1 ERAD complex underlies its diverse client range. J. Cell Biol. *188*, 707–716.

Kim, T.Y., Kim, E., Yoon, S.K., and Yoon, J.B. (2008). Herp enhances ER-associated protein degradation by recruiting ubiquilins. Biochem. Biophys. Res. Commun. *369*, 741–746.

Kim, I., Li, Y., Muniz, P., and Rao, H. (2009). Usa1 protein facilitates substrate ubiquitylation through two separate domains. PLoS ONE *4*, e7604.

Kny, M., Standera, S., Hartmann-Petersen, R., Kloetzel, P.M., and Seeger, M. (2011). Herp regulates Hrd1-mediated ubiquitylation in a ubiquitin-like domain-dependent manner. J. Biol. Chem. *286*, 5151–5156.

Kokame, K., Agarwala, K.L., Kato, H., and Miyata, T. (2000). Herp, a new ubiquitin-like membrane protein induced by endoplasmic reticulum stress. J. Biol. Chem. *275*, 32846–32853.

Leitman, J., Ron, E., Ogen-Shtern, N., and Lederkremer, G.Z. (2013). Compartmentalization of endoplasmic reticulum quality control and ER-associated degradation factors. DNA Cell Biol. *32*, 2–7.

Lerner, M., Corcoran, M., Cepeda, D., Nielsen, M.L., Zubarev, R., Pontén, F., Uhlén, M., Hober, S., Grandér, D., and Sangfelt, O. (2007). The RBCC gene RFP2 (Leu5) encodes a novel transmembrane E3 ubiquitin ligase involved in ERAD. Mol. Biol. Cell *18*, 1670–1682.

Lindquist, S.L., and Kelly, J.W. (2011). Chemical and biological approaches for adapting proteostasis to ameliorate protein misfolding and aggregation diseases: progress and prognosis. Cold Spring Harb. Perspect. Biol. *3*.

McLaughlin, M., Alloza, I., Quoc, H.P., Scott, C.J., Hirabayashi, Y., and Vandenbroeck, K. (2010). Inhibition of secretion of interleukin (IL)-12/IL-23 family cytokines by 4-trifluoromethyl-celecoxib is coupled to degradation via the endoplasmic reticulum stress protein HERP. J. Biol. Chem. *285*, 6960–6969.

Merulla, J., Fasana, E., Soldà, T., and Molinari, M. (2013). Specificity and regulation of the endoplasmic reticulum-associated degradation machinery. Traffic *14*, 767–777.

Miura, H., Hashida, K., Sudo, H., Awa, Y., Takarada-Iemata, M., Kokame, K., Takahashi, T., Matsumoto, M., Kitao, Y., and Hori, O. (2010). Deletion of Herp facilitates degradation of cytosolic proteins. Genes Cells *15*, 843–853.

Molinari, M., Galli, C., Piccaluga, V., Pieren, M., and Paganetti, P. (2002). Sequential assistance of molecular chaperones and transient formation of covalent complexes during protein degradation from the ER. J. Cell Biol. *158*, 247–257.

Monastyrska, I., Ulasli, M., Rottier, P.J., Guan, J.L., Reggiori, F., and de Haan, C.A. (2013). An autophagy-independent role for LC3 in equine arteritis virus replication. Autophagy *9*, 164–174.

Nakatsukasa, K., Brodsky, J.L., and Kamura, T. (2013). A stalled retrotranslocation complex reveals physical linkage between substrate recognition and proteasomal degradation during ER-associated degradation. Mol. Biol. Cell *24*, 1765–1775, S1–S8.

Neutzner, A., Neutzner, M., Benischke, A.S., Ryu, S.W., Frank, S., Youle, R.J., and Karbowski, M. (2011). A systematic search for endoplasmic reticulum (ER) membrane-associated RING finger proteins identifies Nixin/ZNRF4 as a regulator of calnexin stability and ER homeostasis. J. Biol. Chem. *286*, 8633–8643.

Ninagawa, S., Okada, T., Takeda, S., and Mori, K. (2011). SEL1L is required for endoplasmic reticulum-associated degradation of misfolded luminal proteins but not transmembrane proteins in chicken DT40 cell line. Cell Struct. Funct. *36*, 187–195.

Okuda-Shimizu, Y., and Hendershot, L.M. (2007). Characterization of an ERAD pathway for nonglycosylated BiP substrates, which require Herp. Mol. Cell *28*, 544–554.

Pincus, D., and Walter, P. (2012). A first line of defense against ER stress. J. Cell Biol. *198*, 277–279.

Price, J.C., Guan, S., Burlingame, A., Prusiner, S.B., and Ghaemmaghami, S. (2010). Analysis of proteome dynamics in the mouse brain. Proc. Natl. Acad. Sci. USA *107*, 14508–14513.

Reggiori, F., Monastyrska, I., Verheije, M.H., Calì, T., Ulasli, M., Bianchi, S., Bernasconi, R., de Haan, C.A., and Molinari, M. (2010). Coronaviruses Hijack the LC3-I-positive EDEMosomes, ER-derived vesicles exporting short-lived ERAD regulators, for replication. Cell Host Microbe *7*, 500–508.

Sai, X., Kokame, K., Shiraishi, H., Kawamura, Y., Miyata, T., Yanagisawa, K., and Komano, H. (2003). The ubiquitin-like domain of Herp is involved in Herp degradation, but not necessary for its enhancement of amyloid beta-protein generation. FEBS Lett. *553*, 151–156.

Sato, T., Sako, Y., Sho, M., Momohara, M., Suico, M.A., Shuto, T., Nishitoh, H., Okiyoneda, T., Kokame, K., Kaneko, M., et al. (2012). STT3B-dependent posttranslational N-glycosylation as a surveillance system for secretory protein. Mol. Cell *47*, 99–110.

Schulze, A., Standera, S., Buerger, E., Kikkert, M., van Voorden, S., Wiertz, E., Koning, F., Kloetzel, P.M., and Seeger, M. (2005). The ubiquitin-domain protein HERP forms a complex with components of the endoplasmic reticulum associated degradation pathway. J. Mol. Biol. *354*, 1021–1027.

Shmueli, A., Tsai, Y.C., Yang, M., Braun, M.A., and Weissman, A.M. (2009). Targeting of gp78 for ubiquitin-mediated proteasomal degradation by Hrd1: cross-talk between E3s in the endoplasmic reticulum. Biochem. Biophys. Res. Commun. *390*, 758–762.

Stolz, A., Schweizer, R.S., Schäfer, A., and Wolf, D.H. (2010). Dfm1 forms distinct complexes with Cdc48 and the ER ubiquitin ligases and is required for ERAD. Traffic *11*, 1363–1369.

Tcherpakov, M., Delaunay, A., Toth, J., Kadoya, T., Petroski, M.D., and Ronai, Z.A. (2009). Regulation of endoplasmic reticulum-associated degradation by RNF5-dependent ubiquitination of JNK-associated membrane protein (JAMP). J. Biol. Chem. *284*, 12099–12109.

van Laar, T., Schouten, T., Hoogervorst, E., van Eck, M., van der Eb, A.J., and Terleth, C. (2000). The novel MMS-inducible gene Mif1/KIAA0025 is a target of the unfolded protein response pathway. FEBS Lett. *469*, 123–131.

Walter, P., and Ron, D. (2011). The unfolded protein response: from stress pathway to homeostatic regulation. Science *334*, 1081–1086.

Webster, J.M., Tiwari, S., Weissman, A.M., and Wojcikiewicz, R.J. (2003). Inositol 1,4,5-trisphosphate receptor ubiquitination is mediated by mammalian Ubc7, a component of the endoplasmic reticulum-associated degradation pathway, and is inhibited by chelation of intracellular Zn2+. J. Biol. Chem. *278*, 38238–38246.

Weissman, A.M., Shabek, N., and Ciechanover, A. (2011). The predator becomes the prey: regulating the ubiquitin system by ubiquitylation and degradation. Nat. Rev. Mol. Cell Biol. *12*, 605–620.

Ye, Y., Meyer, H.H., and Rapoport, T.A. (2001). The AAA ATPase Cdc48/p97 and its partners transport proteins from the ER into the cytosol. Nature *414*, 652–656.

Younger, J.M., Chen, L., Ren, H.Y., Rosser, M.F., Turnbull, E.L., Fan, C.Y., Patterson, C., and Cyr, D.M. (2006). Sequential quality-control checkpoints triage misfolded cystic fibrosis transmembrane conductance regulator. Cell *126*, 571–582.

Molecular Cell, Volume *52*

Supplemental Information

Autoadaptive ER-Associated Degradation Defines a Preemptive Unfolded Protein Response Pathway

Riccardo Bernasconi, Carmela Galli, Koichi Kokame, and Maurizio Molinari

Molecular Genetics & Genomic Medicine

Open Access

ORIGINAL ARTICLE

Candidate gene analysis using genomic quantitative PCR: identification of *ADAMTS13* large deletions in two patients with Upshaw-Schulman syndrome

Yuka Eura[1], Koichi Kokame[1], Toshiro Takafuta[2], Ryojiro Tanaka[3], Hikaru Kobayashi[4], Fumihiro Ishida[5], Shuichi Hisanaga[6], Masanori Matsumoto[7], Yoshihiro Fujimura[7] & Toshiyuki Miyata[1]

[1]Department of Molecular Pathogenesis, National Cerebral and Cardiovascular Center, Suita, Osaka, Japan
[2]Department of Hematology and Clinical Immunology, Nishi-Kobe Medical Center, Kobe, Hyogo, Japan
[3]Department of Nephrology, Hyogo Prefectural Kobe Children's Hospital, Kobe, Hyogo, Japan
[4]Department of Hematology, Nagano Red Cross Hospital, Nagano, Japan
[5]Department of Biomedical Laboratory Sciences, Shinshu University School of Medicine, Matsumoto, Nagano, Japan
[6]Department of Nephrology, Koga General Hospital, Miyazaki, Japan
[7]Department of Blood Transfusion Medicine, Nara Medical University, Kashihara, Nara, Japan

Keywords
ADAMTS13, genetic analysis, hereditary disease, mutation, quantitative PCR, thrombotic thrombocytopenic purpura, Upshaw-Schulman syndrome

Correspondence
Koichi Kokame, Department of Molecular Pathogenesis, National Cerebral and Cardiovascular Center, Suita, Osaka 565-8565, Japan.
Tel: +81 6 6833 5012; Fax: +81 6 6835 1176; E-mail: kame@ncvc.go.jp

Funding Information
Y. E. was a research resident supported by the Association for Preventive Medicine of Japan at the National Cerebral and Cardiovascular Center. This work was supported in part by grants from the Ministry of Health, Labour, and Welfare of Japan; from the Ministry of Education, Culture, Sports, Science, and Technology of Japan; from Japan Society for the Promotion of Science; and from the Takeda Science Foundation.

Received: 1 November 2013; Revised: 18 December 2013; Accepted: 19 December 2013

doi: 10.1002/mgg3.64

Abstract

Direct sequencing is a popular method to discover mutations in candidate genes responsible for hereditary diseases. A certain type of mutation, however, can be missed by the method. Here, we report a comprehensive genomic quantitative polymerase chain reaction (qPCR) to complement the weakness of direct sequencing. Upshaw-Schulman syndrome (USS) is a recessively inherited disease associated with severe deficiency of plasma ADAMTS13 activity. We previously analyzed *ADAMTS13* in 47 USS patients using direct sequencing, and 44 of them had either homozygous or compound heterozygous mutations. Then, we sought to reveal more extensive defects of *ADAMTS13* in the remaining three patients. We quantified copy numbers of each *ADAMTS13* exon in the patients by using genomic qPCR. Each primer pair was designed to contain at least one of the two primers used in direct sequencing, to avoid missing any exonic deletions. The qPCR demonstrated heterozygous loss of exons 7 and 8 in one patient and exon 27 in the other, and further analysis revealed c.746_987+373del1782 and c.3751_3892+587del729, respectively. Genomic qPCR provides an effective method for identifying extensive defects of the target genes.

Target exon resequencing using direct sequencing is a popular method to discover causative mutations in the candidate genes responsible for hereditary diseases. Homozygous or compound heterozygous mutations are often identified in the corresponding genes of the patients with autosomal-recessive diseases. In some cases, however, only one or no causative mutation is identified in the responsible gene: (an)other mutation(s) may be

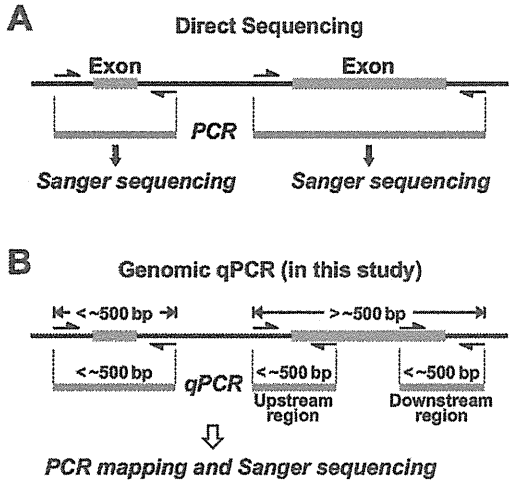

Figure 1. Principles of direct sequencing and genomic qPCR for genetic analysis. (A) In direct sequencing, target regions are amplified by PCR using primer pairs (arrows) usually designed from the intronic sequences flanking each exon, and the PCR products are directly sequenced by the Sanger method. (B) In genomic qPCR, copy numbers of target regions are quantified by real-time PCR. Each primer pair contains at least one of the two primers used in direct sequencing: common primer pairs are used for the regions smaller than ~500 bp, and, for accurate qPCR, one common and one specific primer are used for the regions larger than ~500 bp. If abnormal copy numbers are detected, PCR mapping and sequencing are performed to determine the precise sites of defects.

missed by the method. Although next-generation sequencing may be useful in such cases, it needs special equipments and is still expensive. In this study, we report a comprehensive genomic quantitative PCR (qPCR), which will be a powerful tool in combination with direct sequencing.

Upshaw-Schulman syndrome (USS), also called hereditary thrombotic thrombocytopenic purpura (TTP), is an autosomal-recessive trait associated with severely deficient plasma ADAMTS13 activity. Homozygous or compound heterozygous mutations in the *ADAMTS13* gene (OMIM 604134) are identified in most patients with USS (Levy et al. 2001; Kokame et al. 2002; Kokame and Miyata 2004; Matsumoto et al. 2004; Lotta et al. 2010; Fujimura et al. 2011; Hing et al. 2013). So far, more than 130 causative mutations have been identified by direct sequencing. Using that method, we previously analyzed *ADAMTS13* in 47 Japanese USS patients from 41 unrelated families (Fujimura et al. 2011). Of those, 44 patients from 38 families had either homozygous or compound heterozygous mutations in *ADAMTS13*. In the remaining three patients, however, only single missense mutations (two patients) or no mutation (one patient) was detected. In this study, we sought to reveal more extensive defects of *ADAMTS13* in these three patients by using genomic qPCR.

In general, PCR primer pairs for direct sequencing are designed to hybridize within the intronic sequences flanking each exon (Fig. 1A). Mutations such as substitutions, insertions, and deletions occurring in exons and exon–intron boundaries are identified by Sanger sequencing following genomic PCR, regardless of their heterozygosity or homozygosity (Fig. S1A). Direct sequencing, however, misses heterozygous mutations on the allele that contains no or mismatched primer target sequences: not only whole or partial deletion but also point mutations including single-nucleotide polymorphisms of primer target sequences can hamper PCR-amplification of the mutant allele, which may contain other critical mutations in the exon or exon–intron boundary (Fig. S1B). In these cases, only the target region of the other (normal) allele is PCR-amplified and sequenced, and the results are interpreted as if the regions of both alleles are normal.

Copy number analysis may overcome the limitations of direct sequencing. Multiplex ligation-dependent probe amplification (MLPA) analysis (Schouten et al. 2002) is often used for this purpose. Although MLPA is suitable for detection of genetic defects including exon deletions and duplications, it may still miss mutations that occur outside the probe target sequences. Therefore, to comple-

Figure 2. Genetic analysis of three USS families. (A) Pedigrees and genotypes of the USS patient families. Circles with arrows indicate the probands, USS-W4, -X5, and -KK3. Clinical data of the patients and the basis of diagnosis were described previously (Fujimura et al. 2011); the description of USS-KK3 being the second of three children needs to be corrected. Plasma ADAMTS13 activities were measured by us (USS-W and -X) or by Dr. Miha Furlan at University of Bern in 1999 (USS-KK), and are shown as a percentage of the normal control. ND, not determined. No subjects had ADAMTS13 inhibitors. Squares and circles with numbers indicate the subjects for genetic analysis. Each mutation was assigned a name for cDNA according to the nomenclature recommendations of the HGVS (http://www.hgvs.org/mutnomen/) based on the reference sequences AB069698.2 (cDNA) and NC_000009.11 (genomic). *,§Missense substitutions identified by direct sequencing. †Deletions identified by genomic qPCR in this study. *Pathologically unrelated missense polymorphisms. (B) Identification of exon deletions in *ADAMTS13*. Ct values of genomic qPCR are plotted by dots with lines at the mean (n = 2) for each target region. The letters u and d following the exon numbers indicate upstream and downstream region of each exon, respectively. Red circles, USS-W4; green squares, USS-X5; blue triangles, USS-KK3. Arrows indicate the dots with Ct values higher than those of the other two patients. (C) *Left*: PCR-amplification of the 3.6-kbp band from the normal *ADAMTS13* allele produced a 1.8-kbp band from USS-W4, her mother (W2) and her brother (W3), but not from her father (W1). *Right*: PCR-amplification of the 1.2-kbp band from the normal *ADAMTS13* allele produced a 0.5-kbp band from USS-KK3, but not from her mother (KK2). (D) Sequencing of the 1.8- and 0.5-kbp bands in (C) indicated a 1782-bp deletion in USS-W4 and a 729-bp deletion in USS-KK3, respectively.

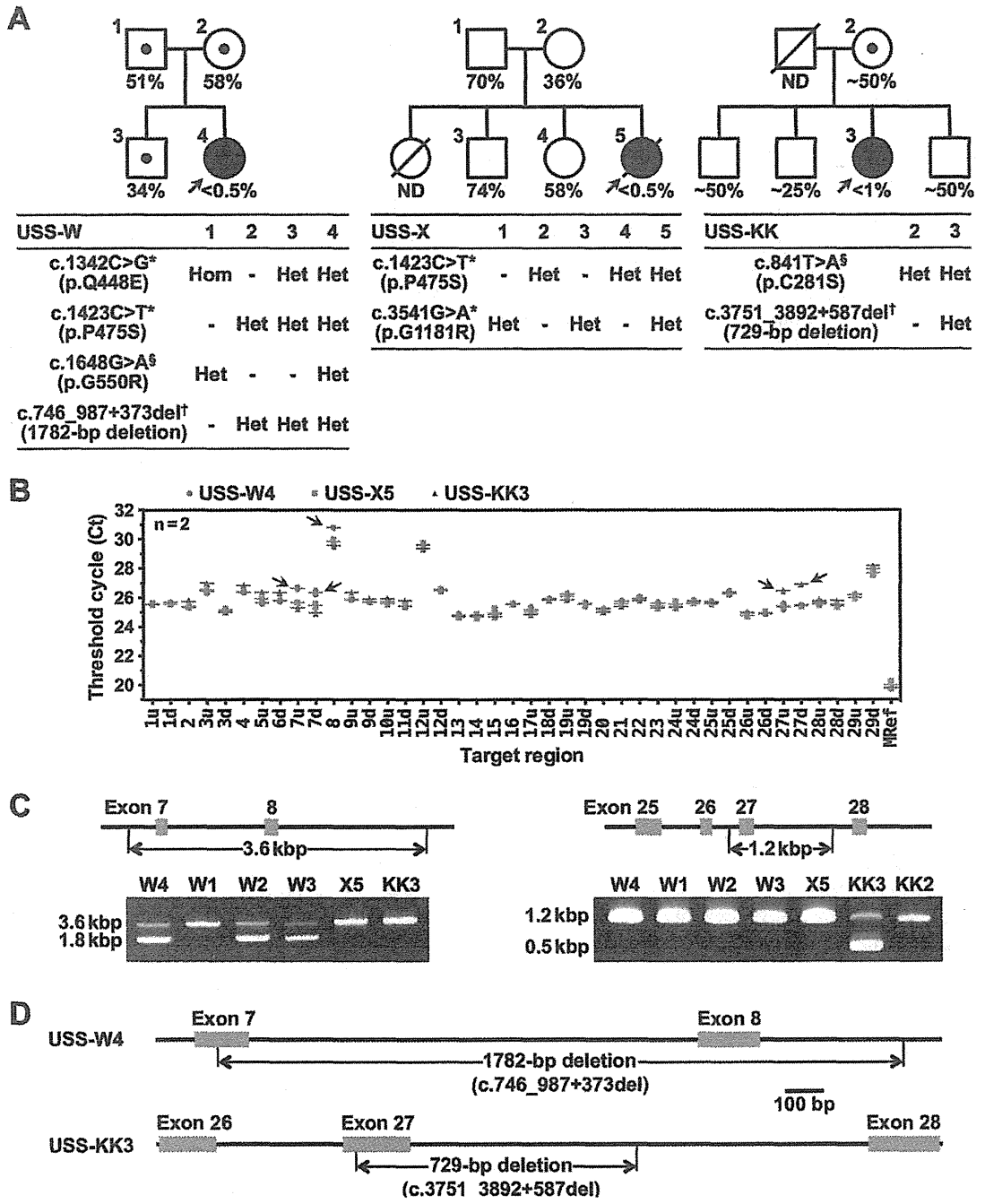

ment direct sequencing, we selected genomic qPCR (Aldape et al. 2002; Kuramitsu et al. 2012), using primer pairs containing at least one of the two primers used in direct sequencing (Fig. 1B). Combining direct sequencing and genomic qPCR should reveal any defects occurring within or between primer target sequences.

The study protocol was approved by the ethical committee of the National Cerebral and Cardiovascular Center; only subjects who provided written informed consent for genetic analyses were included. This study involved three USS families, USS-W, -X, and -KK (Fig. 2A). Clinical data of the patients (USS-W4, -X5, and -KK3) and the basis of diagnosis were described previously (Fujimura et al. 2011). Plasma ADAMTS13 activities for patients and family members are shown in Figure 2A. No subjects had ADAMTS13 inhibitors. The results of direct sequenc-

ing are also shown in Figure 2A. USS-W4 was a heterozygote with paternal c.1648G>A (p.G550R), USS-X5 had no causative mutations, and USS-KK3 was a heterozygote with maternal c.841T>A (p.C281S). Pathologically unrelated missense polymorphisms (p.Q448E, p.P475S, p.G1181R) (Kokame et al. 2011) were also identified in them (Fig. 2A).

Genomic DNA was prepared from blood and subjected to real-time PCR to quantify the copy numbers of each *ADAMTS13* exon. Each primer pair was designed, using Primer-BLAST (NCBI), to contain at least one of two primers used in direct sequencing (Table S1). A primer pair for the qBiomarker Multicopy Reference Copy Number Assay (MRef, Qiagen, Valencia, CA), which recognizes a stable sequence that appears >60 times throughout the human genome, was used to precisely normalize sample DNA input (~4 ng/reaction). PCR was performed using the QuantiFast SYBR Green PCR Kit (Qiagen) for all regions except exon 7 and the KOD SYBR qPCR Mix (Toyobo, Osaka, Japan) for exon 7. Dimethyl sulfoxide was added (final concentration, 5%) for amplification of exon 8. Fluorescence intensities were detected using the Mx3000P QPCR System (Agilent Technologies, Santa Clara, CA), and each threshold cycle (Ct) value was calculated using the MxPro software (Agilent Technologies).

In genomic qPCR, the difference in Ct among subject DNAs is important information. An increase in Ct value of 1.0 indicates a heterozygous deletion of the target region, whereas a decrease of 0.58 indicates a heterozygous duplication. Ct values of the *ADAMTS13* qPCR indicated that exons 7 and 8 were heterozygously absent in USS-W4 and that exon 27 was heterozygously absent in USS-KK3 (Fig. 2B). By contrast, genomic qPCR revealed no abnormalities in USS-X5.

To confirm the deletions and narrow the deleted regions, we performed PCR using primer pairs specific to regions surrounding the deleted exons. Primers 5′-CACCTCCCCACAGACTCCTA-3′ (intron 6) and 5′-AGGCGGGCAAATCATGAGG-3′ (intron 8) amplified a 3.6-kbp band from the normal allele and a 1.8-kbp band from the mutant allele of USS-W4 (Fig. 2C, *left*). Thus, ~1.8 kbp was deleted within the region straddling exons 7 and 8 in USS-W4. The precise sites where the deletions occurred were determined by sequencing the lower PCR band, which revealed that loss of exons 7 and 8 was caused by a 1782-bp deletion ranging from the 60th nucleotide of exon 7 to the 373rd nucleotide of intron 8 (c.746_987+373del1782) (Figs. 2D, S2A). We confirmed the compound heterozygosity of p.G550R and c.746_987+373del1782 in USS-W4 by genomic PCR of the family members. The patient's mother and brother, but not father, had c.746_987+373del1782 (Fig. 2C, *left*). Direct sequencing indicated that the patient's father, but not mother and brother, had p.G550R (Fig. 2A, *left*).

On the other hand, primers 5′-AGTCACATAGCCA GCAGTGG-3′ (intron 26) and 5′-GCACTGAGCAGAG TGGTCTT-3′ (intron 27) amplified a 1.2-kbp band from the normal allele and a 0.5-kbp band from the mutant allele of USS-KK3 (Fig. 2C, *right*). Thus, ~0.7 kbp was deleted within the region straddling exon 27 in USS-KK3. Sequencing the lower band revealed that loss of exon 27 was caused by a 729-bp deletion ranging from the 36th nucleotide of exon 27 to the 587th nucleotide of intron 27 (c.3751_3892+587del729) (Figs. 2D, S2B). Although the patient's father could not be genetically analyzed, her mother had p.C281S (Fig. 2A, *right*), but not c.3751_3892+587del729 (Fig. 2C, *right*). Thus, it was likely that USS-KK3 was a compound heterozygote of p.C281S and c.3751_3892+587del729.

In conclusion, this study identified two USS patients carrying *ADAMTS13* alleles bearing exon deletions. Extensive defects of *ADAMTS13* may be more common than we expect, and genomic qPCR analysis will be effective for identifying such defects in USS patients. Of the three patients we examined, one did not exhibit abnormalities detectable by either direct sequencing or genomic qPCR. Because these combined analytical methods cannot detect large-scale events such as inversions and translocations that do not affect sequences or copy numbers of target regions, the patient may carry such a defect in *ADAMTS13*. Alternatively, plasma ADAMTS13 deficiency in the patient may be brought about by defects other than *ADAMTS13*, for example, genes involved in synthesis, folding, or secretion of ADAMTS13. Finally, we propose well-designed comprehensive genomic qPCR to complement the weakness of direct sequencing of candidate genes.

Acknowledgments

We thank Ayami Isonishi for her technical assistance. Y. E. was a research resident supported by the Association for Preventive Medicine of Japan at the National Cerebral and Cardiovascular Center. This work was supported in part by grants from the Ministry of Health, Labour, and Welfare of Japan; from the Ministry of Education, Culture, Sports, Science, and Technology of Japan; and from Japan Society for the Promotion of Science.

Conflict of Interest

M. M. is a clinical advisory board for Alexion Pharmaceuticals. Y. F. is a clinical advisory board for Baxter Bioscience and for Alexion Pharmaceuticals.

References

Aldape, K., D. G. Ginzinger, and T. E. Godfrey. 2002. Real-time quantitative polymerase chain reaction: a potential tool for genetic analysis in neuropathology. Brain Pathol. 12:54–66.

Fujimura, Y., M. Matsumoto, A. Isonishi, H. Yagi, K. Kokame, K. Soejima, et al. 2011. Natural history of Upshaw-
Schulman syndrome based on *ADAMTS13* gene analysis in Japan. J. Thromb. Haemost. 9(Suppl. 1):283–301.

Hing, Z. A., T. Schiller, A. Wu, N. Hamasaki-Katagiri, E. B. Struble, E. Russek-Cohen, et al. 2013. Multiple in silico tools predict phenotypic manifestations in congenital thrombotic thrombocytopenic purpura. Br. J. Haematol. 160:825–837.

Kokame, K., and T. Miyata. 2004. Genetic defects leading to hereditary thrombotic thrombocytopenic purpura. Semin. Hematol. 41:34–40.

Kokame, K., M. Matsumoto, K. Soejima, H. Yagi, H. Ishizashi, M. Funato, et al. 2002. Mutations and common polymorphisms in *ADAMTS13* gene responsible for von Willebrand factor-cleaving protease activity. Proc. Natl. Acad. Sci. USA 99:11902–11907.

Kokame, K., Y. Kokubo, and T. Miyata. 2011. Polymorphisms and mutations of *ADAMTS13* in the Japanese population and estimation of the number of patients with Upshaw-Schulman syndrome. J. Thromb. Haemost. 9:1654–1656.

Kuramitsu, M., A. Sato-Otsubo, T. Morio, M. Takagi, T. Toki, K. Terui, et al. 2012. Extensive gene deletions in Japanese patients with Diamond-Blackfan anemia. Blood 119:2376–2384.

Levy, G. G., W. C. Nichols, E. C. Lian, T. Foroud, J. N. McClintick, B. M. McGee, et al. 2001. Mutations in a member of the *ADAMTS* gene family cause thrombotic thrombocytopenic purpura. Nature 413:488–494.

Lotta, L. A., I. Garagiola, R. Palla, A. Cairo, and F. Peyvandi. 2010. *ADAMTS13* mutations and polymorphisms in congenital thrombotic thrombocytopenic purpura. Hum. Mutat. 31:11–19.

Matsumoto, M., K. Kokame, K. Soejima, M. Miura, S. Hayashi, Y. Fujii, et al. 2004. Molecular characterization of *ADAMTS13* gene mutations in Japanese patients with Upshaw-Schulman syndrome. Blood 103:1305–1310.

Schouten, J. P., C. J. McElgunn, R. Waaijer, D. Zwijnenburg, F. Diepvens, and G. Pals. 2002. Relative quantification of 40 nucleic acid sequences by multiplex ligation-dependent probe amplification. Nucleic Acids Res. 30:e57.

Supporting Information

Additional Supporting Information may be found in the online version of this article:

Table S1. Primer pairs for *ADAMTS13* genomic qPCR.

Figure S1. Combinatorial analysis of direct sequencing and genomic qPCR should catch any defects occurring on and between the primer target sequences. Direct sequencing detects mutations such as point mutations (including substitutions, insertions, and deletions), short insertions, and deletions in the exons and exon–intron boundaries (A), but misses mutations on the allele that contains no or mismatched primer target sequences (B). Genomic qPCR for quantifying the copy numbers of target regions complements the results of direct sequencing.

Figure S2. Deleted regions and flanking sequences of *ADAMTS13* identified in two patients with USS. The 1782- and 729-bp regions (red letters) were deleted in patients USS-W4 (A) and USS-KK3 (B), respectively. Lowercase and uppercase sequences indicate introns and exons, respectively. Underlined sequences adjacent to the breakpoints may cause microhomology-mediated end joining (MMEJ) (McVey and Lee. Trends Genet. 2008;24:529–538).

基礎研究

ADAMTS13と血栓性血小板減少性紫斑病

小亀浩市

はじめに

難病（厚生労働省が難治性疾患克服研究事業の対象としている疾患）の一つに血栓性血小板減少性紫斑病（thrombotic thrombocytopenic purpura：TTP）がある。血小板減少症と溶血性貧血を呈し，時に腎障害や精神神経障害，発熱を併発する疾患で，長いあいだ原因不明とされてきた。その病態はO157等の病原性大腸菌感染による溶血性尿毒症症候群（hemolytic uremic syndrome：HUS）と類似しており，両者とも血栓性微小血管障害症（thrombotic microangiopathy：TMA）に属する。von Willebrand factor（VWF）切断酵素ADAMTS13の存在が明らかになって以来，TTPに関する研究は飛躍的に進展した。本稿では，ADAMTS13研究に初期から携わってきた筆者らの成果を中心に，TTP研究の進歩を紹介する。

Key word
ADAMTS13
von Willebrand factor
血小板
血栓
血栓性血小板減少性紫斑病

ADAMTS13 and thrombotic thrombocytopenic purpura

Koichi Kokame :
Department of Molecular Pathogenesis, National Cerebral and Cardiovascular Center Research Institute
国立循環器病研究センター研究所 分子病態部

Ⅰ．TTPの初報告からADAMTS13の発見まで

16歳の少女が突然に全身性の症状に襲われ，数日で死に至った経過が1924年に報告された[1]。病理検査で諸臓器の細小動脈に硝子様血栓が観察されたことなどを踏まえ，TTPの最初の報告とされている。その約60年後，TTP患者の血漿に異常に高分子量化したVWFが存在すること[2]や，TTPの血栓はVWFを多く含むこと[3]が示された。

なぜ患者血漿に異常高分子量VWFが存在するのかという疑問は，血漿のVWF切断活性を測定する方法の発明[4,5]で解決に向かい，VWF切断酵素の活性低下がTTP発症の原因となると予想された。そして数年後，VWF切断酵素の精製とcDNAクローニングが報告された[6,7]。一方，先天性TTP患者家系の遺伝子連鎖解析が行われ，責任遺伝子としてADAMTS13が同定された[8]。VWF切断酵素とADAMTS13の一次構造が完全に一致したことで，TTP＝ADAMTS13欠損症という概念が生まれ，TTPの分子病態研究が本格化した。

Ⅱ．VWFとADAMTS13とTTPの関係

止血反応の初期には，血小板凝集が起こる。VWFは，血小板同士の結合を橋渡しする重要なタンパク質である。主に血管内皮細胞や骨髄巨核球で合成され，ポリペプチド鎖（モノマー）が数十個，直鎖状に共有結合した巨大マルチマー（＞20,000kDa）として分泌され

る。分子量が大きいほど，血小板凝集能は高い。通常，ADAMTS13で適度に切断されて500～15,000kDaという分子量分布で存在するが，何らかの理由でADAMTS13の活性が失われると異常高分子量VWFマルチマーが残存する。異常高分子量VWFマルチマーは血小板を過剰に凝集させるため，細小血管に血栓が生じる（図1）。TTPの病態は，以下のように説明できる。過剰凝集により血小板が消費されると循環血液中の血小板数は減少し（血小板減少症），血栓で生じた血管狭窄部位を通過することで赤血球は破砕される（溶血性貧血）。多数の血栓で腎臓の細小血管が閉塞すると腎機能が障害され，大脳の細小血管が閉塞すると精神神経障害が起こる。

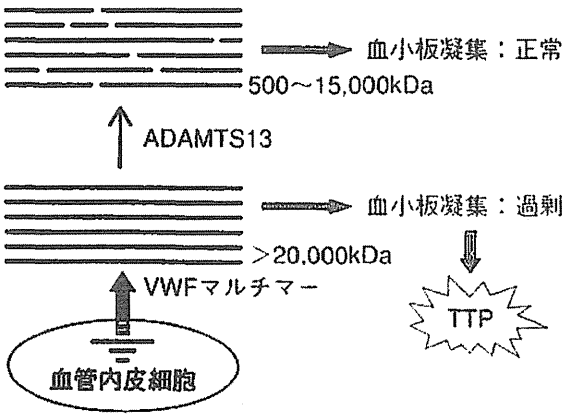

図1．TTPの発症メカニズム

TTPは，先天性と後天性に分類される。先天性TTPはUpshaw-Schulman syndrome（USS）とも呼ばれ，ADAMTS13遺伝子異常を原因とする劣性遺伝様式の疾患である。一方，後天性TTPではADAMTS13活性に対する阻害性抗体が生じていることが多く，そのため，自己免疫疾患の一種と言うことができる。

Ⅲ．ADAMTS13の構造

ADAMTS13は，その名が示す通りADAMTSファミリー（ヒトの場合19遺伝子）に属する亜鉛型メタロプロテアーゼである。主に肝臓の星細胞で合成され，1,427アミノ酸残基，分子量約190kDaで，多くの構造単位を持つ（図2）。VWFを切断するにはMドメインからSドメインまでが必須であり，それよりC末端側部分は*in vitro*の反応系では必要ない。我々は，VWF認識に重要なDドメインからSドメインまでの立体構造をX線解析で決定した[9]。その結果，予想外にもDドメインはディスインテグリン様の構造ではないこと，CドメインとDドメインの骨格構

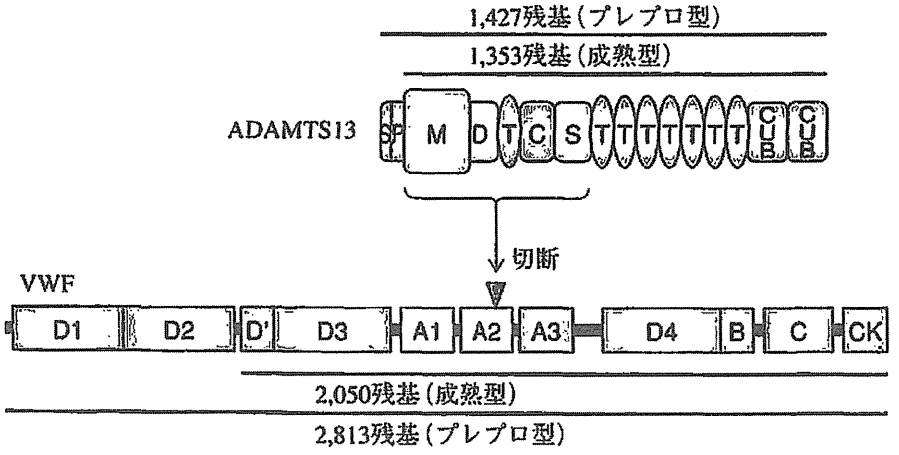

図2．ADAMTS13およびVWFのドメイン構成

造は相同であること，Sドメインは球状構造であること，空間的に離れた3カ所のVWF結合エキソサイトが直線状に並んでいることなど，様々な特徴を明らかにした。基本構造はADAMTSファミリー内で保存されていると考えられるので，複数のエキソサイトを介した基質認識機構はADAMTS分子に共通の特性であると予想された。事実，ADAMTS5でも類似の基質認識機構が示唆された[10]。

Ⅳ．ADAMTS13によるVWFの切断

VWFも，複数のドメイン構造からなる（図2）。血管損傷部位の内皮下組織（コラーゲン）と血小板の結合あるいは血小板同士の結合には，主にA1およびA3ドメインが直接関与する。ADAMTS13が切断するのはA2ドメインであるが，その切断部位は分子内部に埋もれており，そのままではADAMTS13は接近できない。VWFが血小板に結合し，血流によって発生するずり応力が加わると，VWFは部分的に伸展し，切断部位が表面に現れる（図3）。これでADAMTS13が，A2ドメインを切断できるようになる。このことは，ADAMTS13によってVWFを*in vitro*で切断させる際，タンパク質変性剤の共存，あるいはボルテックス等による強い撹拌を必要とすることと一致する。ずり応力でA2ドメインがほぐれ，新たに露出した領域がADAMTS13の複数のエキソサイトと広範囲で相互作用することで，VWFの切断が生理的条件下で特異的かつ調節的に起こると考えられる。つまり，生理的には，VWFにかかるずり応力の強さが切断反応を調節し，血小板凝集の程度をうまく制御するのかもしれない。

Ⅴ．VWF73を用いたADAMTS13活性測定

ADAMTS13はVWFのTyr^{1605}～Met^{1606}間を切断するが，その反応においてADAMTS13とVWFは互いの分子構造を広範囲で認識する。ADAMTS13が活性を発揮するにはMドメインからSドメインまでが必須であり，一方，

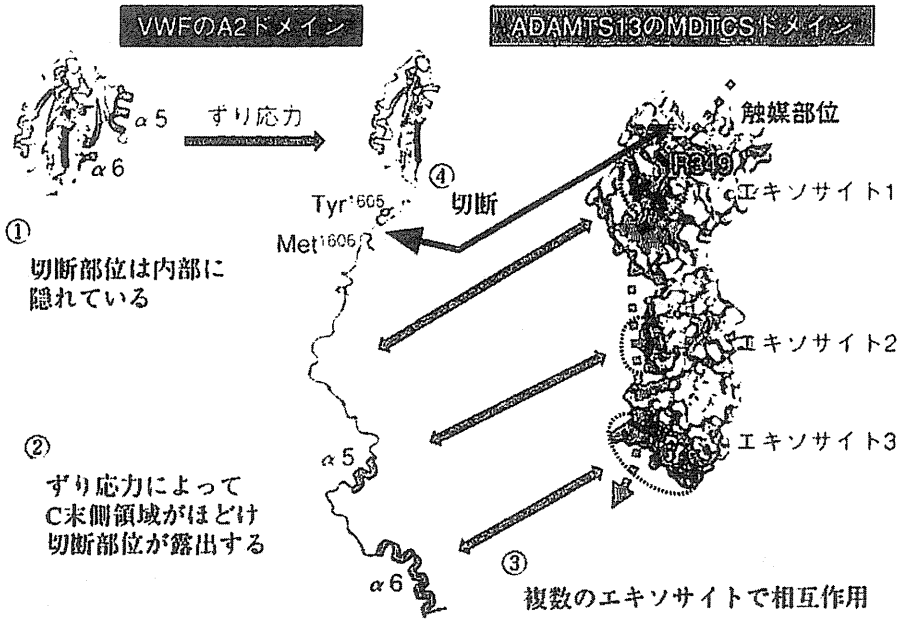

図3．ADAMTS13によるVWFの切断

VWF側ではA2ドメインに含まれる73アミノ酸残基（Asp^{1596}～Arg^{1668}：VWF73と呼ぶ）が必要十分であることを明らかにした（特許取得）[11]。VWF全長を基質として利用する従来の活性測定法は，いずれも操作が煩雑などの理由で臨床検査として普及しなかったが，VWF73を利用した測定法はいくつも開発され，なかでも我々が開発したFRET法[12]とAct-ELISA法[13]は研究および臨床の場に普及している。

FRET法では，化学合成ペプチドFRETS-VWF73を基質として用いる。ADAMTS13で切断される前は，切断部位の両側に付加された蛍光基と消光基の間で蛍光共鳴エネルギー転移（fluorescence resonance energy transfer：FRET）が起こるため，基質溶液に励起光を照射しても蛍光は弱い。ADAMTS13によって切断されると，FRET効果が緩和されて蛍光が強くなる（図4）。したがって，蛍光強度の増大を観察することでADAMTS13の活性を検出することができる。Act-ELISA法では，VWF73がADAMTS13で切断されて生じる末端部分のみに結合するモノクローナル抗体を利用する。96ウェルプレートにGST-VWF73融合タンパク質を結合させ，ここに血漿を添加して切断反応を行う。HRP標識した上述の抗体を添加するとウェル上のGST-VWF73断片に定量的に結合するので，発色基質で検出する（図4）。

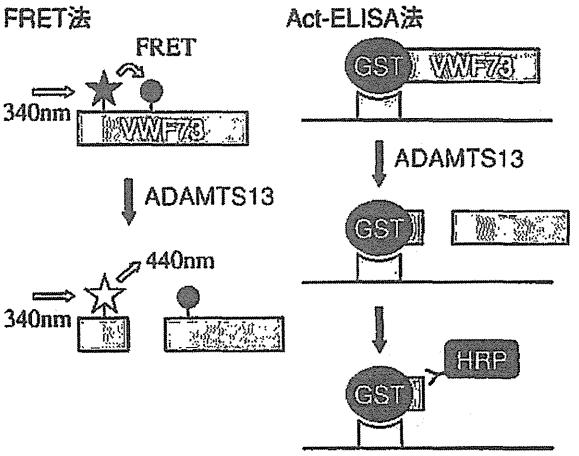

図4. FRET法およびAct-ELISA法によるADAMTS13活性測定

Ⅵ. 先天性TTP患者の遺伝子解析

先天性TTP（＝USS）はADAMTS13欠損症であり，患者はADAMTS13遺伝子異常の複合ヘテロあるいはホモ接合体である。我々は奈良県立医科大学と共同で，日本人USS患者の遺伝子解析を行っている[14-16]。これまでUSS患者47名（41家系）を解析し，44名（38家系）に複合ヘテロあるいはホモの原因変異を同定した。世界的には130を超える原因変異が報告されているが，我々の報告は，その4割近くを占める。全例において，ダイレクトシークエンシング法が用いられている。変異の種類としてはミスセンス変異が最も多いが，ナンセンス変異やフレームシフト変異，スプライシング異常なども同定されている。エクソン全体の欠失や，遺伝子全体の欠失あるいは転座といった大きな領域の異常はまだ報告されていない。我々は最近，原因変異を特定できていなかった患者に対し，プライマーデザインを工夫した定量PCRによるコピー数解析を行い，729塩基および1,782塩基の欠失を見つけた（Eura et al，論文投稿中）。ADAMTS13だけでなく全ての遺伝子に適用可能な方法なので，普及（宣伝）に努めたい。

Ⅶ. 日本人のADAMTS13遺伝子多型と活性

我々は日本人一般住民のADAMTS13遺伝子解析を行い，健常者にも見出されるミスセンス多型として，T339R，Q448E，P475S，P618A，S903L，G1181Rを同定した[14,17]。これらがUSS患者に見つかっても原因変異とは考えない。ただし，P475SはADAMTS13

の活性を少し低下させる[14, 18, 19]。韓国人および中国人にも存在するが，欧米人には見られない多型である。現在のところ，ADAMTS13遺伝子多型と疾患との関連は見出されていない。

国立循環器病研究センターで1989年から実施されている一般住民を対象とした吹田研究の一部として，3,616人の血漿ADAMTS13活性を測定した[20]。男性のADAMTS13活性平均値は女性に比べて有意に低く，男女とも60歳台以上で徐々に低下した。一方，VWF量は加齢によって増加するため，血栓傾向の指標となるVWF量/ADAMTS13活性比では加齢に伴う増加傾向が顕著に現れた。ABO血液型がO型の人は他に比べてVWF量が低いが，ADAMTS13活性は血液型と有意な相関を示さなかった。

Ⅷ．先天性TTP患者数の推定

日本に，先天性TTP患者は何人いるのか。類似疾患の多い，希少な遺伝性疾患の患者数を明らかにすることは意外に難しい。浸透率（遺伝子異常を持っている場合に発症する率）が不明なので，先天性ADAMTS13欠損者数＝先天性TTP患者数とは言えないが，吹田研究の活性データと遺伝子解析データを組み合わせて，先天性ADAMTS13欠損者数の推定を試みた[17]。その結果，いくつかの前提条件を仮定すれば，日本人の先天性ADAMTS13欠損症者（複合ヘテロあるいはホモ接合体）の頻度は約100万人に1人と推定された。これがどのくらい正確か分からないが，これまでに日本で同定されたUSS患者が50人程であることを考えると妥当な数である。

Ⅸ．マウスのADAMTS13

我々はマウスADAMTS13のcDNAをクローニングし，遺伝子構造を明らかにした[21]。さらに，ADAMTS13欠損マウスを作製し表現型を解析した[22]。先天性ADAMTS13欠損患者と同様，マウスでも血中に異常高分子量VWFマルチマーが存在した。しかし，先天性TTPモデルとして作製したにもかかわらず，予想した血小板減少や溶血性貧血は見られなかった。つまり，マウスにおいてはADAMTS13完全欠損以外の要因がTTP発症に必要であった。その後，ヒトにおいてもADAMTS13欠損だけではTTPを発症せず，内皮障害や妊娠など他の要因が加わって症状が顕在化する場合もあることが分かった。ADAMTS13欠損マウスは自然にTTPを発症しないとは言え，潜在的な血栓形成傾向は示した。同時期に米国のグループも欠損マウスを作製しており，通常飼育下でTTP症状は見られないが，血中VWF量が高い系統への戻し交配により一部の個体にTTP様症状が出現することを報告した[23]。我々が作製したADAMTS13欠損マウスは，脳虚血再還流障害モデル[24]や急性心筋梗塞モデル[25]などに利用されている。

マウスでは，系統特異的に2種類のADAMTS13が発現する[21]。129/Sv系統のADAMTS13遺伝子は，ヒトと同様，29個のエクソンからなり，ドメイン構成もヒトと同じである。一方，BALB/c，C3H/He，C57BL/6，DBA/2系統では，イントロン23にレトロトランスポゾン配列が挿入しており，7番目のTドメイン以降を欠失したADAMTS13が発現する。これを利用して，ADAMTS13のC末端領域は高ずり応力下での血小板血栓形成を抑制するために機能することを証明した[26]。

おわりに

ここに述べたように，ADAMTS13やVWFの解析を通じてTTPの研究がかなり進んだ。ADAMTS13活性測定法の進歩で診断が正確

になったことは，基礎研究が実用化に結びついた好例と言える。TTPの治療には，ADAMTS13補充を目的として新鮮凍結血漿が使用されているが，現在，組換えADAMTS13製剤の開発が進んでおり，治療法の改善も期待できる。反面，ADAMTS13活性の低下が顕著でないTTP症例や，ADAMTS13活性低下が目立つHUSなど，発症機序を明確に説明できない病態も存在する。非典型溶血性尿毒症症候群（atypical HUS：aHUS）や深部静脈血栓症（deep vein thrombosis：DVT）とADAMTS13の関連も詳しく調べる価値があろう。ADAMTS13によるVWF切断機構にもまだ不明の部分があり，興味深い知見も得られつつある。これからの研究の進展が楽しみである。

本稿で紹介した成果は，国立循環器病研究センター分子病態部の宮田敏行部長をはじめとした研究室構成員，病院の小久保喜弘医長や宮田茂樹医長，奈良県立医科大学の藤村吉博教授，松本雅則准教授，化血研の副島見事博士など，多くの方々との共同研究で得られたものであり，ここに感謝の意を表します。

§ 文 献

1）Moschcowitz E : Hyaline thombosis of the terminal arterioles and capillaries ; a hitherto undescribed disease. Proc NY Pathol Soc 1924;24:21-4.
2）Moake JL, Rudy CK, Troll JH et al : Unusually large plasma factor VIII : von Willebrand factor multimers in chronic relapsing thrombotic thrombocytopenic purpura. N Engl J Med 1982;307(23):1432-5.
3）Asada Y, Sumiyoshi A, Hayashi T, et al : Immunohistochemistry of vascular lesion in thrombotic thrombocytopenic purpura, with special reference to factor VIII related antigen. Thromb Res 1985;38(5):469-79.
4）Furlan M, Robles R, Lämmle B : Partial purification and characterization of a protease from human plasma cleaving von Willebrand factor to fragments produced by in vivo proteolysis. Blood 1996;87(10):4223-34.
5）Tsai HM : Physiologic cleavage of von Willebrand factor by a plasma protease is dependent on its conformation and requires calcium ion. Blood 1996;87(10):4235-44.
6）Soejima K, Mimura N, Hirashima M, et al : A novel human metalloprotease synthesized in the liver and secreted into the blood : possibly, the von Willebrand factor-cleaving protease?. J Biochem 2001;130(4):475-80.
7）Zheng X, Chung D, Takayama TK, et al : Structure of von Willebrand factor-cleaving protease (ADAMTS13), a metalloprotease involved in thrombotic thrombocytopenic purpura. J Biol Chem 2001;276(44):41059-63.
8）Levy GG, Nichols WC, Lian EC, et al : Mutations in a member of the ADAMTS gene family cause thrombotic thrombocytopenic purpura. Nature 2001;413(6855):488-94.
9）Akiyama M, Takeda S, Kokame K, et al : Crystal structures of the noncatalytic domains of ADAMTS13 reveal multiple discontinuous exosites for von Willebrand factor. Proc Natl Acad Sci USA 2009;106(46):19274-9.
10）Gao W, Zhu J, Westfield LA, et al : Rearranging exosites in noncatalytic domains can redirect the substrate specificity of ADAMTS proteases. J Biol Chem 2012;287(32):26944-52.
11）Kokame K, Matsumoto M, Fujimura Y, et al : VWF73, a region from D1596 to R1668 of von Willebrand factor, provides a minimal substrate for ADAMTS-13. Blood 2004;103(2):607-12.
12）Kokame K, Nobe Y, Kokubo Y, et al : FRETS-VWF73, a first fluorogenic substrate for ADAMTS13 assay. Br J Haematol 2005;129(1):93-100.
13）Kato S, Matsumoto M, Matsuyama T, et al : Novel monoclonal antibody-based enzyme immunoassay for determining plasma levels of ADAMTS13 activity. Transfusion 2006;46(8):1444-52.
14）Kokame K, Matsumoto M, Soejima K, et al : Mutations and common polymorphisms in ADAMTS13 gene responsible for von Willebrand factor-cleaving protease activity. Proc Natl Acad Sci USA 2002;99(18):11902-7.
15）Fujimura Y, Matsumoto M, Isonishi A, et al : Natural history of Upshaw-Schulman syndrome based on ADAMTS13 gene analysis in Japan. J

Thromb Haemost 2011;9(Suppl 1):283-301.
16) Kokame K, Aoyama Y, Matsumoto M, et al : Inherited and de novo mutations of ADAMTS13 in a patient with Upshaw-Schulman syndrome. J Thromb Haemost 2008;6(1):213-5.
17) Kokame K, Kokubo Y, Miyata T : Polymorphisms and mutations of ADAMTS13 in the Japanese population and estimation of the number of patients with Upshaw-Schulman syndrome. J Thromb Haemost 2011;9(8):1654-6.
18) Akiyama M, Kokame K, Miyata T : ADAMTS13 P475S polymorphism causes a lowered enzymatic activity and urea lability in vitro. J Thromb Haemost 2008;6(10):1830-2.
19) Akiyama M, Nakayama D, Takeda S, et al : Crystal structure and enzymatic activity of an ADAMTS-13 mutant with the East Asian-specific P475S polymorphism. J Thromb Haemost 2013;11(7):1399-406.
20) Kokame K, Sakata T, Kokubo Y, et al : von Willebrand factor-to-ADAMTS13 ratio increases with age in a Japanese population. J Thromb Haemost 2011; 9(7):1426-8.
21) Banno F, Kaminaka K, Soejima K, et al : Identification of strain-specific variants of mouse Adamts13 gene encoding von Willebrand factor-cleaving protease. J Biol Chem 2004;279(29):30896-903.
22) Banno F, Kokame K, Okuda T, et al : Complete deficiency in ADAMTS13 is prothrombotic, but it alone is not sufficient to cause thrombotic thrombocytopenic purpura. Blood 2006;107(8):3161-6.
23) Motto DG, Chauhan AK, Zhu G, et al : Shigatoxin triggers thrombotic thrombocytopenic purpura in genetically susceptible ADAMTS13-deficient mice. J Clin Invest 2005;115(10):2752-61.
24) Fujioka M, Hayakawa K, Mishima K, et al : ADAMTS13 gene deletion aggravates ischemic brain damage : a possible neuroprotective role of ADAMTS13 by ameliorating postischemic hypoperfusion. Blood 2010;115(8):1650-3.
25) Doi M, Matsui H, Takeda H, et al : ADAMTS13 safeguards the myocardium in a mouse model of acute myocardial infarction. Thromb Haemost 2012; 108(6):1236-8.
26) Banno F, Chauhan AK, Kokame K, et al : The distal carboxyl-terminal domains of ADAMTS13 are required for regulation of in vivo thrombus formation. Blood 2009;113(21):5323-9.